

Crystallographic texture approximation by quadratic programming

Thomas Böhlke^{a,*}, Utz-Uwe Haus^b, Volker Schulze^c

^a *Otto-von-Guericke-Universität Magdeburg, Institut für Mechanik, PSF 4120, 39016 Magdeburg, Germany*

^b *Otto-von-Guericke-Universität Magdeburg, Institut für Mathematische Optimierung, PSF 4120, 39016 Magdeburg, Germany*

^c *Volkswagen AG, EZVT Methodenplanung/Umformsimulation, Brieffach 179612, Germany*

Received 12 August 2005; received in revised form 24 October 2005; accepted 9 November 2005

Available online 19 January 2006

Abstract

This paper considers the problem of approximating a given crystallite orientation distribution function (codf) by a set of texture components. Problems of this type arise for example if the codf has to be reconstructed from discrete orientations or if one looks for a physical interpretation of the codf. The same problem is encountered if crystallographic texture based constitutive models have to be specified. The equivalence of these tasks to a mixed integer quadratic programming problem (MIQP) – a standard but challenging problem in optimization theory – is shown. Special emphasis is given to the generation of a class of approximations with an increasing number of texture components. Furthermore, the constraints resulting from the non-negativity, the normalization, and the symmetry of the codf are analyzed. Finally, a set of approximations of three different experimental textures determined with this solution scheme is presented and discussed. Based on these hierarchical solutions, the engineer can decide in what detail the microstructure is considered.

© 2005 Acta Materialia Inc. Published by Elsevier Ltd. All rights reserved.

Keywords: Crystallographic texture; One-point correlation function of crystal orientations; Orientation distribution function; Quadratic programming; Texture components

1. Introduction

Single phase polycrystals are composed of grains of the same material which differ with respect to their lattice orientations. The simplest statistical description of such microstructures is based on the crystallite orientation distribution function (codf) which specifies the volume fraction of a material having a specific lattice orientation. The codf is the one-point correlation function of lattice orientation and describes the crystallographic texture in the material. Higher-order correlation functions allow for a description of the morphological texture. The correlation functions can be estimated based on orientation data determined experimentally for example by X-ray diffraction or by automated electron backscatter diffraction orientation measurements. For a review concerning the representation of microstructures of polycrys-

tals and the experimental determination of their mesoscale microstructure see Adams and Olson [1].

Due to the general complexity of a codf it is often necessary to look for simplified, but physical, descriptions which are essentially low dimensional. In the context of crystallographic textures this was first done by Wasserman and Grewen [38], who introduced so called texture components to describe textures peculiar to specific processing histories. A large amount of work has been done to formulate isotropic and anisotropic model functions and to identify the dominant components in experimental textures [22,17,16]. Texture components are used on the one hand to obtain a physical interpretation of experimental codfs and on the other hand to homogenize the mechanical behavior with an acceptable numerical effort. Taylor type material models [35,37,25,6,28] allow for a description of the macroscopic mechanical behavior due to a specific slip system geometry and orientation distribution. From the numerical point of view, large scale finite element simulations of metal forming operations based on the Taylor

* Corresponding author.

E-mail addresses: boehlke@mb.uni-magdeburg.de (T. Böhlke), haus@mail.math.uni-magdeburg.de (U.-U. Haus), volker.schulze@volkswagen.de (V. Schulze).

model are very time-intensive and storage-consuming if the crystallographic texture is approximated by several hundred discrete crystals. Therefore, Raabe and Roters [30] introduced the so called texture component crystal plasticity method which describes crystallographic textures by small sets of discrete orientations. Due to the discontinuous approximation of the codf the approach by Raabe and Roters [30] requires a random variation of the discrete crystal orientation through the sample. In the approach by Böhlke et al. [4] texture components are described by continuous model functions. The effective stress is obtained by integrating the crystal stress – weighted by the codf – over the orientation space. The two material models mentioned before require an approximation of the codf by discrete or continuous texture components. The method suggested in this paper yields both a discrete (taking only the main orientations into account) and a continuous approximation, in the last case also giving a rigorous error bound.

In some applications, the codf is already discretized into a finite set of weighted orientations. If the number of orientations needs to be reduced, the proposed method can be used to find an optimal set of components to approximate the initial distribution.

In this paper we restrict our attention to the formulation as a mixed integer quadratic programming problem (MIQP) problem and its approximate solution without considering mechanical properties. These could only be predicted based on several simplifications and assumptions which themselves are still a subject under discussion. For the case of a continuous approximation of the codf a discussion of effective mechanical properties can be found for example in Refs. [4,5].

The outline of the paper is as follows. After a short review of existing approximation techniques in Section 2, the basic features of the codf and its properties implied by crystal and sample symmetries are discussed in Sections 3 and 4. The concept of texture components is introduced in Section 5 and specified for the case of the von Mises–Fisher–Matthies distribution function, widely used in texture analysis. Section 6 deals with the problem of approximating a codf by a set of model functions. Special emphasis is given to constraints resulting from the requirement of an approximation with a small number of texture components. It is shown that such a problem is equivalent to a definite mixed integer quadratic programming problem (MIQP). Optimization problems of such a type arise in rather different contexts such as chemical process optimization and portfolio optimization. Finally, in Section 7 the approximation of three different experimental textures based on this solution scheme is considered. It is shown that the applied solution procedure yields good approximations in terms of quality and quantity.

2. Previous approaches

The problem of finding approximations for a given texture has been considered in detail by Kocks et al. [20], Toth

and Van Houtte [36], and Helming et al. [18]. The earliest approach for discretizing a given codf was to put a nearly equidistant grid on the Euler space in a $90^\circ \times 90^\circ \times 90^\circ$ region. For each of the so defined boxes the codf is integrated and the respective volume fraction is determined. Since the resulting number of boxes is usually too high for a subsequent simulation, boxes with a volume fraction above a specified limit are selected and renormalized as the approximation of the codf. This cutting technique (CUT) has been analyzed and criticized by Toth and Van Houtte [36]. The same authors suggest two new discretization schemes in order to improve the CUT method. The first (statistical) method (STAT) is based on a cumulative orientation distribution function which is used to map random numbers onto the orientation space such that for a large set of these numbers the texture is reproduced. The cumulative function is generated again based on a grid with a characteristic resolution. The only parameter of the algorithm (beside the aforementioned resolution) is the number of random orientations used for the approximation. The second technique – called the limited orientation distance (LOD) method – is also based on a grid on the orientation space. Intensities on grid points are transferred to points with higher intensities if the distance between the points is smaller than a specific value. The two parameters of this algorithm are the mesh size and the distance which governs the transfer. The authors analyze and compare both methods with respect to the (i) reproducibility of the codf, (ii) the prediction of effective mechanical properties, (iii) the prediction of deformation textures based on these discretization, and (iv) the effect of rediscrizations during deformation texture modeling. It is shown that both methods are superior to the CUT method and that the LOD technique works better for the high intensity regions whereas the STAT method is better in regions where the intensity is low. The earlier approach by Kocks et al. [20] used a random grid on the orientations space and assigns suitable weights in an iterative procedure.

A special approach for the approximation of steel textures was developed by Delannay et al. [11]. In this approach the texture is characterized by a set of parameters, describing typical features of industrial steel sheets by prescribed fibers. The parameters vary the intensities, the fiber thickness and the position of the knots controlling the fibers. Another approach with standardized positions and components is given by Cho et al. [9]. In this paper the approximation is performed on a set of typical components for cubic metals. The components are located at fixed points and described by von Mises–Fisher distributions with fixed half-widths. The weight of the component is calculated similar to the LOD technique: the volume fraction of a component is equal to the sum of all intensities within a certain acceptance angle. These special approximation techniques depend strongly on the expertise of the user and are only suited to a special class of textures.

As an alternative a genetic approach by Tarasiuk et al. [34] for identifying the texture components may also be mentioned. However, such methods can by design never

guarantee global optimality of their solution, and do not provide an error bound which would be of help in evaluating their quality.

3. The crystallite orientation distribution function

A crystal orientation is described by a proper orthogonal tensor $\mathbf{Q} = \mathbf{g}_i \otimes \mathbf{e}_i \in SO(3)$ which is introduced in such a way that it maps the fixed reference basis \mathbf{e}_i onto the lattice vectors \mathbf{g}_i . \mathbf{Q} can be parameterized by Euler angles $\phi_1 = \varphi_1$, $\phi_2 = \Phi$, $\phi_3 = \varphi_2$ [8]

$$(\mathbf{Q}^\top)_{ij} = \begin{bmatrix} C_1 C_3 - S_1 C_2 S_3 & S_1 C_3 + C_1 C_2 S_3 & S_2 S_3 \\ -C_1 S_3 - S_1 C_2 C_3 & -S_1 S_3 + C_1 C_2 C_3 & S_2 C_3 \\ S_1 S_2 & -C_1 S_2 & C_2 \end{bmatrix}, \quad (1)$$

where C_i and S_i denote the values $\cos(\phi_i)$ and $\sin(\phi_i)$, respectively. The matrix components refer to the base vectors \mathbf{e}_i . The transposition is introduced in order to make the description of crystal orientations by $\mathbf{Q} = \mathbf{g}_i \otimes \mathbf{e}_i$ compatible to the one introduced by Bunge [8].

The codf $f(\mathbf{Q})$ specifies the volume fraction dv/v of crystals having the orientation \mathbf{Q} [7,31], i.e.

$$\frac{dv}{v}(\mathbf{Q}) = f(\mathbf{Q})dQ, \quad (2)$$

dQ is the volume element in $SO(3)$ which ensures an invariant integration over $SO(3)$ [14], i.e.

$$\int_{SO(3)} f(\mathbf{Q})dQ = \int_{SO(3)} f(\mathbf{Q}\mathbf{Q}_0)dQ \quad \forall \mathbf{Q}_0 \in SO(3). \quad (3)$$

If $SO(3)$ is parameterized by Euler angles, the volume element dQ is given by

$$dQ = \frac{\sin(\Phi)}{8\pi^2} d\varphi_1 d\Phi d\varphi_2. \quad (4)$$

The function $f(\mathbf{Q})$ is non-negative and normalized such that

$$f(\mathbf{Q}) \geq 0 \quad \forall \mathbf{Q} \in SO(3), \quad \int_{SO(3)} f(\mathbf{Q})dQ = 1. \quad (5)$$

The orientation distribution function $f(\mathbf{Q})$ reflects both the symmetry of the crystallites forming the aggregate and the sample symmetry, which results from the processing history. The crystal symmetry implies the following symmetry relation for $f(\mathbf{Q})$

$$f(\mathbf{Q}) = f(\mathbf{Q}\mathbf{H}^C) \quad \forall \mathbf{H}^C \in S^C \subseteq SO(3), \quad (6)$$

where S^C denotes the symmetry group of the crystallite. Similarly, the sample symmetry implies

$$f(\mathbf{Q}) = f(\mathbf{H}^S\mathbf{Q}) \quad \forall \mathbf{H}^S \in S^S \subseteq SO(3). \quad (7)$$

Here S^S denotes the symmetry group of the sample.

4. Elementary regions due to crystal and sample symmetries

The parameterization of the $SO(3)$ with Euler angles results in a periodic space with a natural period of 2π in

all parameters. This periodic cell consists of two equivalent asymmetric units, since a glide plane perpendicular to $\Phi = \pi$ with glide increments of π in φ_1 and φ_2 exists inherently in this parameterization [8]. Therefore a complete presentation of the Euler space is given by either one of the asymmetric units, for example

$$0 \leq \varphi_1 < 2\pi, \quad 0 \leq \Phi < \pi, \quad 0 \leq \varphi_2 < 2\pi. \quad (8)$$

The application of the crystal and sample symmetry operations results in a further reduction of the independent region. The cubic group consists of 24 proper orthogonal transformations resulting in 24 equivalent units within the range given by Eq. (8). In Fig. 1 a typical representation of three anisotropic regions in a φ_1 -cut for cubic crystals is shown [15].

These three prismatic regions are the result of the threefold symmetry axis at $\varphi_2 = \pi/4$; $\Phi = \arccos(\sqrt{3}/3)$ of cubic crystals, which results in a non-linear transformation within the Euler space. For the evaluation of the codf, the region 3 can be problematic since the singular plane with $\Phi = 0$ is included. Region 2 consists of two prismatic parts connected only at the location of the threefold symmetry axis. Therefore the region 1 of Fig. 1 is favorable for an identification procedure. This region is given by

$$0 \leq \varphi_1 < 2\pi, \quad \Phi_l \leq \Phi < \frac{\pi}{2}, \quad 0 \leq \varphi_2 < \frac{\pi}{2}, \quad (9)$$

where

$$\Phi_l = \arccos \min \left(\frac{\cos(\varphi_2)}{\sqrt{1 + \cos^2(\varphi_2)}}, \frac{\sin(\varphi_2)}{\sqrt{1 + \sin^2(\varphi_2)}} \right). \quad (10)$$

In the case of orthorhombic sample symmetry, which consists of a symmetry group of four elements, a reduction in the φ_1 -range to one quarter of the cubic case is possible. Considering the same arguments as before, one elementary region is given by

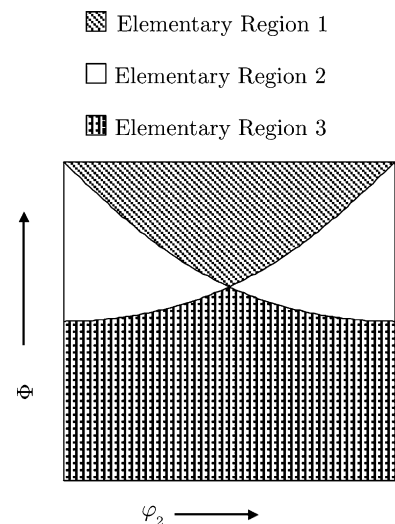


Fig. 1. Elementary regions in a φ_1 -cut for cubic crystals (Φ , $\varphi_2 \in [0, \pi/2]$) [15].

$$0 \leq \varphi_1 < \frac{\pi}{2}, \quad \Phi_l \leq \Phi < \frac{\pi}{2}, \quad 0 \leq \varphi_2 < \frac{\pi}{2}. \quad (11)$$

5. Texture components

Crystallographic textures can often be described by a small number of texture components or texture fibers [38,8,21]. A texture component is a crystal orientation for which the codf shows a (local) maximum in the elementary region. In the neighborhood, the codf is decreasing in an isotropic or anisotropic way. A commonly used model function, which describes a central distribution, is the von Mises–Fisher distribution. The von Mises–Fisher distribution has the maximum entropy of all orientation distributions on $SO(3)$ with the expectation value of \mathbf{Q} equal to \mathbf{Q}_α . This distribution function was introduced by von Mises in a two-dimensional case and by Fisher in a three-dimensional case [23]. Matthies [26] was the first to apply the von Mises–Fisher distribution in texture analysis. He called it a normal distribution in the orientation space see also [27], but this interpretation was criticized by Schaeben [32,33]. Eschner [12] and Eschner and Fundenberger [13] used non-central distribution functions for the description of experimental crystallographic textures. An overview of central and non-central distribution functions on $SO(3)$ can be found in the monograph by Mardia and Jupp [23].

In the following the codf $f(\mathbf{Q})$ is approximated by a set of M model functions $g_\alpha(\mathbf{Q})$ ($\alpha \in \{1, \dots, M\}$) and an isotropic background $g_0(\mathbf{Q}) = 1 \forall \mathbf{Q} \in SO(3)$. The model functions are taken to be central distributions $g_\alpha(\mathbf{Q}) = g(\mathbf{Q}, \mathbf{Q}_\alpha, b_\alpha)$ at \mathbf{Q}_α with half-widths b_α and with weights v_α . We can hence approximate $f(\mathbf{Q})$ by a convex combination of the model functions $g_\alpha(\mathbf{Q})$:

$$f(\mathbf{Q}) \approx \bar{f}(\mathbf{Q}) = \sum_{\alpha=0}^M v_\alpha g(\mathbf{Q}, \mathbf{Q}_\alpha, b_\alpha) \quad (12)$$

with

$$\sum_{\alpha=0}^M v_\alpha = 1, \quad v_\alpha \geq 0 \quad \forall \alpha \in 0, \dots, M. \quad (13)$$

The value of a central distribution $g(\mathbf{Q}, \mathbf{Q}_\alpha, b_\alpha)$ at \mathbf{Q} depends only on the distance ω between \mathbf{Q} and \mathbf{Q}_α , which is generally given by

$$\omega(\mathbf{Q}, \mathbf{Q}_\alpha) = \arccos\left(\frac{1}{2}(\text{tr}(\mathbf{Q}\mathbf{Q}_\alpha^{-1}) - 1)\right) \quad (14)$$

[8]. The von Mises–Fisher distribution is given by

$$g(\mathbf{Q}, \mathbf{Q}_\alpha, b_\alpha) = N(S_\alpha) \exp(S_\alpha \cos(\omega(\mathbf{Q}, \mathbf{Q}_\alpha))), \quad (15)$$

where

$$N_\alpha = \frac{1}{I_0(S_\alpha) - I_1(S_\alpha)} \quad (16)$$

and

$$S_\alpha = S(b_\alpha) = \frac{\ln(2)}{2 \sin^2(b_\alpha/4)}. \quad (17)$$

The modified Bessel functions I_n are defined by

$$I_n(S) = \frac{1}{\pi} \int_0^\pi \exp(S \cos(t)) \cos(nt) dt. \quad (18)$$

As mentioned before, the distribution function $f(\mathbf{Q})$ reflects both the symmetry of the crystallites forming the aggregate and the sample symmetry. The following modified von Mises–Fisher distribution implies the fulfillment of the constraint due to the crystal symmetry

$$g(\mathbf{Q}, \mathbf{Q}_\alpha, b_\alpha) = \frac{1}{24} \sum_{\beta=1}^{24} N_\alpha \exp(S_\alpha \cos(\omega(\mathbf{Q}\mathbf{H}_\beta^C \mathbf{Q}_\alpha^{-1}))), \quad (19)$$

where the $\mathbf{H}_\beta^C \in SO(3)$ are the 24 elements of the symmetry group of cubic crystals. Considering the sample symmetry for the orthorhombic case, the model function can be rewritten as

$$g(\mathbf{Q}, \mathbf{Q}_\alpha, b_\alpha) = \frac{1}{96} \sum_{\beta=1}^{24} \sum_{\gamma=1}^4 N_\alpha \exp(S_\alpha \cos(\omega(\mathbf{H}_\gamma^S \mathbf{Q}\mathbf{H}_\beta^C \mathbf{Q}_\alpha^{-1}))) \quad (20)$$

with the four elements of the orthorhombic group $\mathbf{H}_\gamma^S \in SO(3)$.

6. Identification of the model functions

In the following an approximation $\bar{f}(\mathbf{Q})$ (see Eq. (12)) of $f(\mathbf{Q})$ is defined based on a set of M grid points on the elementary region. Each grid point represents the center of a von Mises–Fisher distribution. To each component a half-width b_α and a volume fraction v_α is assigned. The half-widths b_α of the components are assumed to be identical for all components. The aim is to identify $\bar{f}(\mathbf{Q})$ in terms of the volume fractions v_α such that $\bar{f}(\mathbf{Q})$ approximates the original codf $f(\mathbf{Q})$ with a small number $M_0 \leq M$. This number $M_0 \leq M$ is limited by the computational effort of the application in which the approximation is used. For example in the case of finite element simulation of deep drawing processes the current computational power of the computers limits the total number of components to about 100 in the orientation space.

As a definition of the distance between the two functions $f(\mathbf{Q})$ and $\bar{f}(\mathbf{Q})$ we define

$$D = \int_{SO(3)} (f(\mathbf{Q}) - \bar{f}(\mathbf{Q}))^2 d\mathbf{Q}. \quad (21)$$

The distance D can be reformulated in the following setting

$$D = I - 2 \sum_{\alpha=1}^M v_\alpha h_\alpha + \sum_{\alpha, \beta=1}^M v_\alpha v_\beta G_{\alpha\beta}, \quad (22)$$

where I denotes the texture index

$$I = \int_{SO(3)} f(\mathbf{Q})^2 d\mathbf{Q}. \quad (23)$$

The vector h_α and the matrix $G_{\alpha\beta}$ are given by

$$h_\alpha = \int_{SO(3)} f(\mathbf{Q}) g_\alpha(\mathbf{Q}) d\mathbf{Q}, \quad (24)$$

$$G_{\alpha\beta} = \int_{SO(3)} g_\alpha(\mathbf{Q}) g_\beta(\mathbf{Q}) d\mathbf{Q}. \quad (25)$$

In order to perform the integration over $SO(3)$ (see Eqs. (24) and (25)) the parameterization of $SO(3)$ is changed. Instead of using $\{\varphi_1, \Phi, \varphi_2\}$ the new variable ζ is introduced by $\Phi = \arccos(\zeta)$. Then the metric becomes homogeneous and an integral over $SO(3)$ is given by

$$\int_{SO(3)} f(\mathbf{Q}) \psi(\mathbf{Q}) d\mathbf{Q} = \frac{1}{8\pi^2} \int_0^{\varphi_2^u} \int_0^{\varphi_1^u} \int_{\zeta^l}^{\zeta^u} f(\varphi_1, \Phi(\zeta), \varphi_2) \times \psi(\varphi_1, \Phi(\zeta), \varphi_2) d\varphi_1 d\zeta d\varphi_2 \quad (26)$$

with

$$\varphi_1^u = 2\pi \quad \zeta^l = -1 \quad \zeta^u = +1 \quad (27)$$

and

$$\varphi_2^u = 2\pi \quad \Phi(\zeta) = \arccos(\zeta). \quad (28)$$

Due to the cubic crystal symmetry and the orthorhombic sample symmetry the range of integration can be reduced to $[0, \pi/2]^3$. In that range a Gaussian quadrature scheme is applied with 36 Gauss points in each direction.

Using these definitions it is apparent that we have to solve a quadratic programming problem (QP), namely

$$\min \quad -2 \sum_{\alpha=1}^M v_\alpha h_\alpha + \sum_{\alpha, \beta=1}^M v_\alpha v_\beta G_{\alpha\beta} \quad (29)$$

$$\text{subject to} \quad \sum_{\alpha=1}^M v_\alpha = 1 \quad v_\alpha \geq 0 \quad \forall \alpha \in \mathcal{M}$$

with $\mathcal{M} = \{1, \dots, M\}$ and the additional restriction that at most M_0 of the variables v_α may be positive in the solution. We can model this requirement by introducing M binary variables s_α which are to be 1 if $v_\alpha > 0$. This can be accomplished by the constraints $s_\alpha \geq v_\alpha$. Adding the set packing constraint $\sum_{\alpha=1}^M s_\alpha \leq M_0$ now guarantees that at most M_0 volume fractions are positive, i.e. non-zero, in a solution. The problem of identifying $\bar{f}(\mathbf{Q})$ is thus solved by the MIQP:

$$\begin{aligned} \min \quad & -2 \sum_{\alpha=1}^M v_\alpha h_\alpha + \sum_{\alpha, \beta=1}^M v_\alpha v_\beta G_{\alpha\beta} \\ \text{subject to} \quad & s_\alpha \geq v_\alpha \\ & \sum_{\alpha=1}^M v_\alpha = 1 \\ & \sum_{\alpha=1}^M s_\alpha \leq M_0 \\ & v_\alpha \geq 0 \quad \forall \alpha \in \mathcal{M} \\ & s_\alpha \in \{0, 1\} \quad \forall \alpha \in \mathcal{M} \end{aligned} \quad (30)$$

Note that the matrix $G_{\alpha\beta}$ is by its definition positive definite. The problem (29) as well as its variant with an upper bound on the number of positive variables (30) is of a

similar structure to the well-known question of evaluating risk versus reward in the context of a portfolio of financial assets first described by Markowitz [24]. A successful computational study of the latter has been performed by Bienstock [3]. The significant difference of Eq. (30) in comparison to the instances arising in portfolio optimization is that the matrix G has full rank. Therefore the solution of the problem turns out to be much more difficult than the typical financial problems: the individual QP problems are solved slower, and the number of nodes that must be visited in the branch-and-bound tree is high.

Various reliable methods are available for solving the quadratic programming problem (29), namely Newton-type feasible descent methods, Lagrange-multiplier methods, logarithmic barrier methods, and primal-dual interior point methods. For an overview see Bertsekas [2]. The latter two classes are particularly suited to the definite quadratic programming problems we are dealing with. The mixed-integer quadratic programming problems like (30) are in general much harder to solve than their continuous counterparts, and one can often only resort to branch-and-bound methods.

7. Numerical examples

As an illustration of the outlined procedure, a fit of three typical automotive deep drawing steel grades is performed. Due to the final steps of the manufacturing process of steel sheets, which consist of cold rolling and subsequent annealing, the materials have practically orthorhombic sample symmetry. The measurement of the codf was performed by means of a pole figure measurement with X-ray diffraction on three lattice planes and a subsequent recalculation of the codf using the series expansion method [8] up to $L = 22$.

The first example is DX53, a mild deep drawing steel grade. This material is dominated by a fiber texture close to the γ -fiber, which is given in Euler angles by $(0^\circ \leq \varphi_1 < 90^\circ; \Phi = 54.7^\circ, \varphi_2 = 45^\circ)$. In Fig. 2(a) the measured codf of the material is shown. The other material is a high-strength micro-alloyed steel grade, H340LAD. In this case, the dominant structure is the α -fiber, which is located at $(\varphi_1 = 0^\circ; 0^\circ \leq \Phi < 90^\circ, \varphi_2 = 45^\circ)$, whereas the γ -fiber is less pronounced. The measured codf is given in Fig. 3(a). Beside the differences in the dominant fiber directions, the materials have significantly different peak values.

Both textures were fitted with a grid of 5° within the elementary region by components with a half-width of $b_\alpha = 6^\circ$. For a reduction of the processed data, a preliminary selection of the ansatz functions is performed. For the optimization procedure, only grid points are considered, which have an intensity that is higher than a certain limit value, similar to the CUT method. This preliminary data reduction is performed only to reduce the subsequent processing time, it is not a mandatory part of the approximation process. For this example, the limit was set to 50% of the maximum value of the measured codf. This limits the

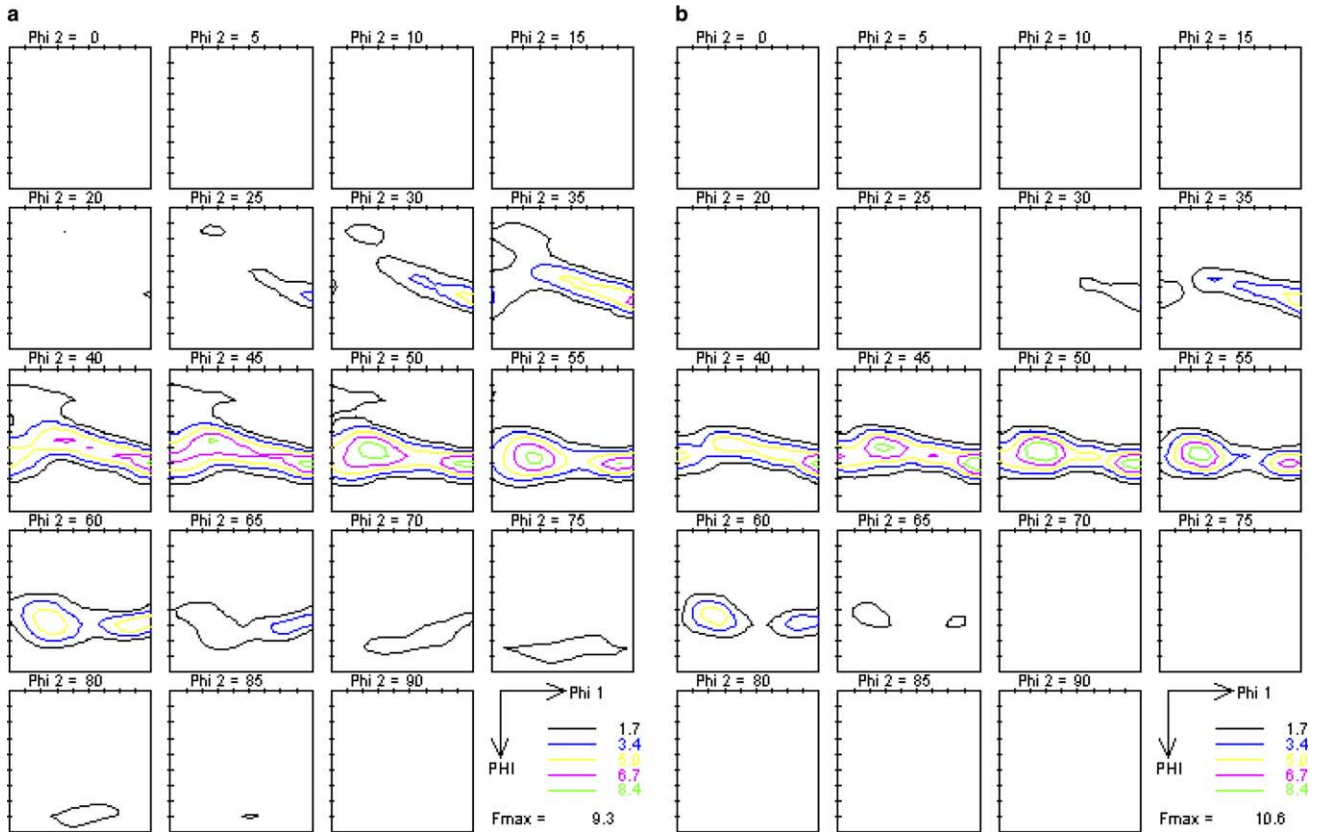


Fig. 2. Texture measurement and approximation with 24 components of DX53. (a) Measurement and (b) approximation.

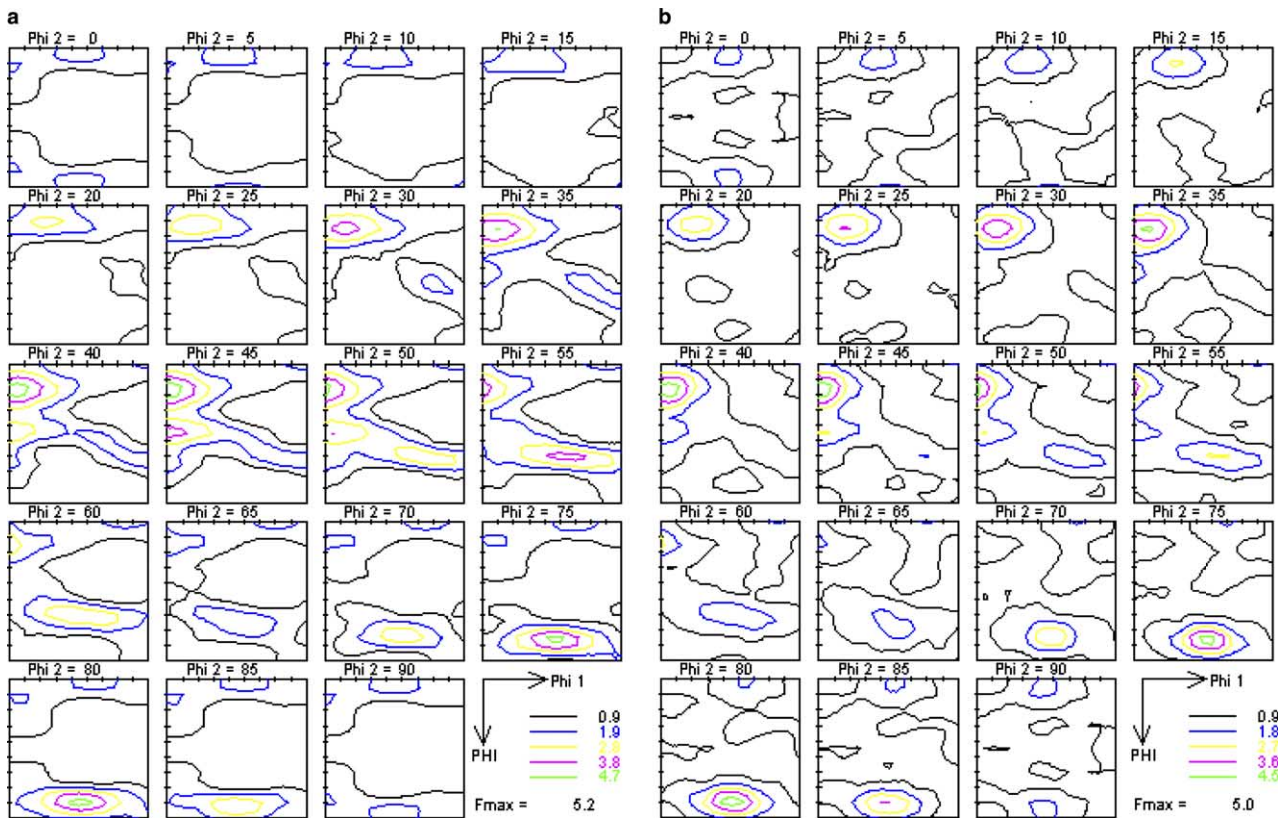


Fig. 3. Texture measurement and approximation with 24 components of H340LAD. (a) Measurement and (b) approximation.

number of ansatz functions to $M = 95$ in case of DX53 and $M = 92$ in case of H340LAD. Within this set of ansatz functions, the optimization with respect to an optimum weight for a given number M_0 of functions is performed.

We used the commercial solver software CPLEX [19] which employs a logarithmic barrier algorithm to solve the initial quadratic optimization problems within less than 6 s on a 1.2 GHz Ultrasparc-IV processor. In addition, for each material a sequence of instances of type (30) was generated, the limit M_0 on the number of positive variables varying between 1 and 24. Solving these instances to optimality using CPLEX within reasonable computation time was impossible except for the smallest instances. However, using solver settings that employ heuristics to find good solutions early in the solution process (`mip emphasis 3` and `mip strategy variableselect 3`), we were able to identify a series of good solutions together with proven bounds on their maximum optimality gap. We also tested the Xpress [10] solver, but found it to be inferior, especially in application to the MIQP problems.

The result of the optimization process is a number of components and their respective weights that approximate the given texture. For these examples, a number of such representations was selected starting with one component up to 24 components, given by the model function of Eq. (20). For a better comparison, cuts along two important directions, the α -fiber and a cut at ($0^\circ \leq \varphi_1 < 90^\circ$, $\varphi_1 = 55^\circ$; $\Phi = 55^\circ$, $\varphi_2 = 55^\circ$) were chosen for the evaluation of the approximated codf. In these cuts, the dominant components of both textures are located or intersecting. The results are presented in Fig. 4 for the DX53 and in Fig. 5 for the H340LAD. In both cases the first component fits the maximum peak of the measured codf. With every additional component, the approx-

imation of the measured distribution improves with an increasing number of ansatz functions. The intensity of the major components is reduced and secondary features start to develop, which can be observed especially in the case of H340LAD.

Using only the identified major components, the resulting texture is too anisotropic, therefore the values of the codf are overestimated in the peak regions. The approximation improves if the information about the remaining isotropic part is also used in the fit. The introduction of this additional component is seamless both in Eqs. (29) and (30), where no decision variable needs to be introduced for it. With this “isotropic” component added to the texture approximation, the dominant values are in the range of the measured texture. In the Figs. 4 and 5 this result is plotted for the case of 24 components next to the measured texture.

In Figs. 2(b) and 3(b) the codf plots for the fitted textures with 24 components and the isotropic part are presented. The comparison with the measured codf shows that not only the dominant components are reproduced but also that the structure of the secondary regions is approximated sufficiently, when the isotropic part is included in the approximation result.

One of the advantages of using MIQP techniques to solve these problems is that an error bound is available at any time: during the course of the branch-and-bound algorithm QP relaxations for the remaining subproblems are solved. The worst objective value among them is then a safe lower bound for the original problem. Fig. 6 illustrates the development of the gap between the objective function value for the best known solution (after 100,000 nodes of branch-and-bound) and the lower bound at that time, for both DX53 and H340. The absolute value of

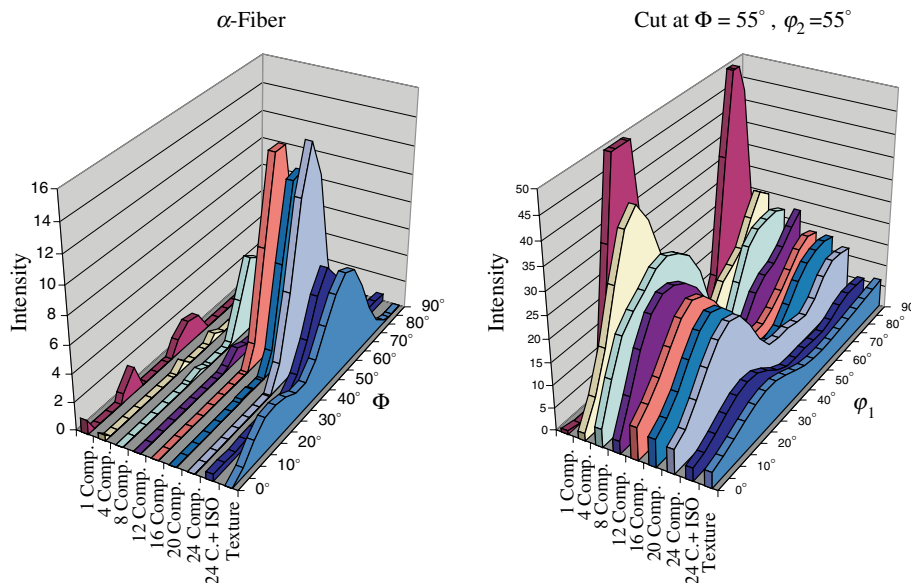


Fig. 4. Approximation of DX53.

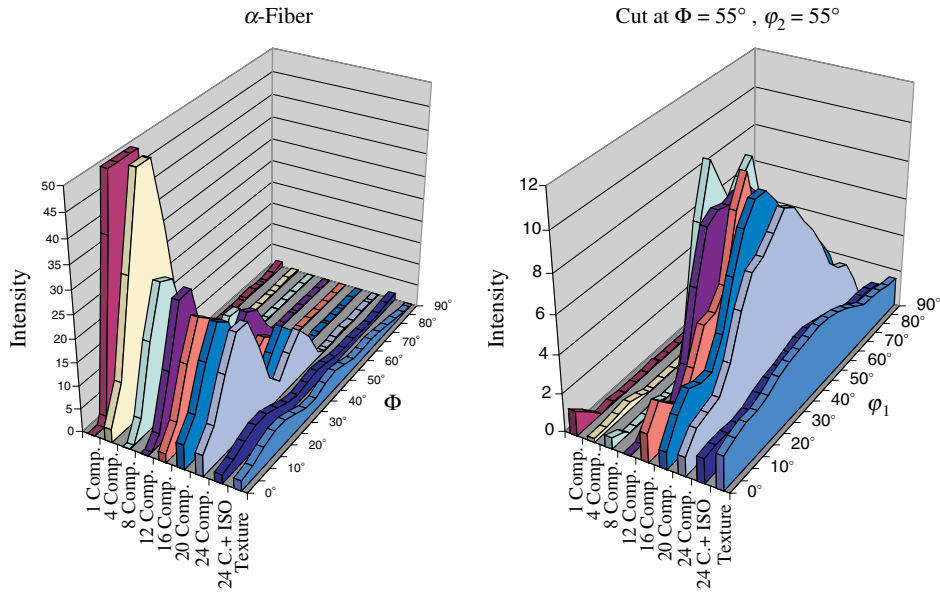


Fig. 5. Approximation of H340LAD.

the slope for the graph of the solutions is smaller for H340, indicating that the weaker texture is harder to approximate with few components.

As a last example, the case of H220PD is considered. This material is a phosphorus-alloyed steel with a good formability and an intermediate strength. The texture measurement (Fig. 7(a)) shows a dominant fiber structure close to the γ -fiber. A secondary feature is the branching of this fiber in the vicinity of the α -fiber. For the approximation, a limit was set to 20% of the maximum intensity, resulting in $M = 250$ ansatz functions. The QP problem (Eq. 29) for this material can be solved within 0.5 s. With varying component limit $M_0 \in \{1, \dots, 24\}$, and limited to 100,000 nodes of branch-and-bound, the MIQP problems took on average 4500 s. The approximation with 24 components is given in Fig. 7(b).

The main components of the fiber structure are reproduced well, but the branching is not reproduced. This effect is caused by the limitation of the number M_0 of ansatz functions. The procedure described above fits the ansatz functions to the main components of the texture. The examples above showed that this approximation improved with an increasing number of components, also reproducing secondary texture features. To approximate more complex textures with a small set of functions, one can introduce an additional requirement: volume fractions selected in a solution of Eq. (30) should not be clustered too closely. The criterion selected was that the spherical angle, given by Eq. (14) between any two volume fractions present in a solution of Eq. (30) should be at least 7.5° . Note that this imposes a stable set or node packing condition on the volume fractions: Define a graph containing all volume fractions as nodes, with two nodes α and β connected by an edge if $\sphericalangle(\mathbf{Q}_\alpha, \mathbf{Q}_\beta) \leq 7.5^\circ$. Then we can model the additional constraints using the edge-node formulation of the stable set polytope [29]:

$$s_\alpha + s_\beta \leq 1 \quad \text{for each pair } (\alpha, \beta) \text{ with } \sphericalangle(\mathbf{Q}_\alpha, \mathbf{Q}_\beta) \leq 7.5^\circ. \quad (31)$$

Introducing this distance criterion, the selected components are forced to a wider distribution, resulting in a better approximation of the secondary features (Fig. 7(c)). The spread in the weights v_α increases to a factor of three between the smallest and the largest weight in the set. Since the volume fraction of the isotropic component v_0 is dominated by the regions of low intensities, the peak values are underestimated. The addition of the stable set conditions increases computation time significantly, to an average 6830 s over the 24 instances considered.

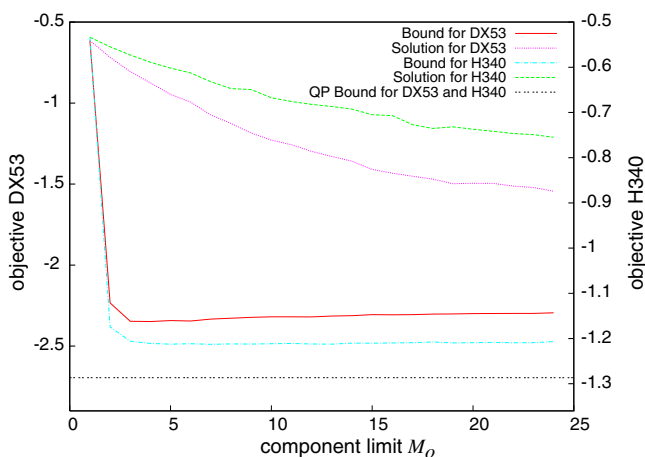


Fig. 6. Error estimation for DX53 and H340LAD.

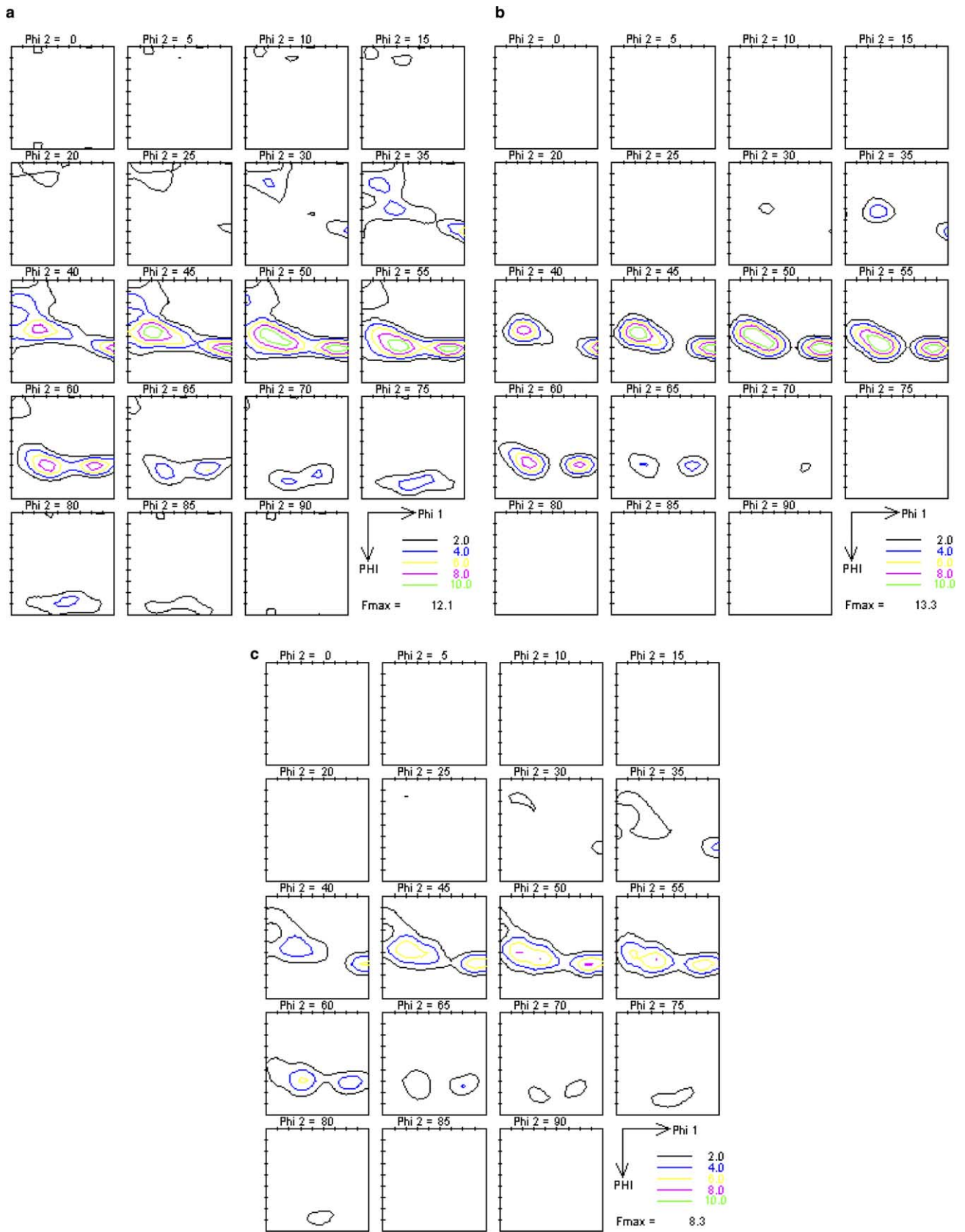


Fig. 7. Texture measurement and approximation of H220PD. (a) Measurement; (b) approximation without distance criterion; (c) approximation with distance criterion.

8. Summary

We have presented a method to approximate a texture with a hierarchical set of texture components using a solution scheme based on the (semidefinite) mixed integer quadratic programming method. This approach is not limited to a special texture class nor to a specific sample or crystal symmetry configuration. The procedure enables the identification of an optimum combination of ansatz functions for a prescribed number M_0 of components in a set. If the computation is stopped prematurely, an error bound for the current state of the approximation is given.

A fitting of typical steel textures with a small number of components was performed. The approximation reproduces the measured textures with a tendency to cluster in regions of high intensities. If a wider distribution of the ansatz functions is needed, a distance based discrimination procedure can be added, which improves the approximation of secondary texture features.

Acknowledgments

T. Böhlke acknowledges the partial support rendered by the Deutsche Forschungsgemeinschaft (DFG) under grant GK 828. U.-U. Haus was supported by grant FOR-468 of the Deutsche Forschungsgemeinschaft. V. Schulze acknowledges the support by the Volkswagen PhD-program.

References

- [1] Adams B, Olson T. The mesostructure-properties linkage in polycrystals. *Progr Mater Sci* 1998;43:1–88.
- [2] Bertsekas DP. *Non-linear programming*. Belmont, MA: Athena Scientific; 1995.
- [3] Bienstock D. Computational study of a family of mixed-integer quadratic programming problems. *Math Program* 1996;74(2):121–40.
- [4] Böhlke T, Risy G, Bertram A. A texture component model for anisotropic polycrystal plasticity. *Computat Mater Sci* 2005;32:284–93.
- [5] Böhlke T, Risy T, Bertram A. A texture based model for polycrystal plasticity. In: *Proceedings of the 14th international conference on textures of materials (ICOTOM-14)*; 2005.
- [6] Bronkhorst C, Kalidindi S, Anand L. Polycrystalline plasticity and the evolution of crystallographic texture in fcc metals. *Roy Soc Lond A* 1992;341:443–77.
- [7] Bunge H-J. *Zur Darstellung allgemeiner Texturen*. *Z Metallkd* 1965;56:872–4.
- [8] Bunge H-J. *Texture analysis in material science*. Göttingen: Cuvillier Verlag; 1993.
- [9] Cho J-H, Rollett AD, Oh KH. Determination of volume fractions of texture components with standard distributions in euler space. *Metall Mater Trans A* 2004;35A:1075–86.
- [10] Dash Optimization, 1999–2004. Dash optimization. Available from: <http://www.dashoptimization.com/>.
- [11] Delannay R, Van Houtte P, Van Bael A, Vanderschueren D. Application of a texture parameter model to study planar anisotropy of rolled steel sheets. *Model Simul Mater Sci Eng* 2000;8:413–22.
- [12] Eschner T. Texture analysis by means of model functions. *Text Microstruct* 1993;21:139–46.
- [13] Eschner T, Fundenberger J. Application of anisotropic texture components. *Text Microstruct* 1997;28:181–95.
- [14] Gel'fand I, Minlos R, Shapiro Z. *Representations of the rotation and Lorentz groups and their applications*. Oxford: Pergamon Press; 1963.
- [15] Hansen J, Pospiech J, Lücke K. *Tables for texture analysis of cubic crystals*. Berlin: Springer; 1978.
- [16] Helming K. *Texturapproximation durch Modellkomponenten*. Göttingen: Cuvillier Verlag; 1996.
- [17] Helming K, Eschner T. A new approach to texture analysis of multiphase materials using a texture component model. *Cryst Res Technol* 1990;25:K203–8.
- [18] Helming K, Schwarzer R, Rauschenbach B, Geier S, Leiss LB, Wenk H-R, et al. Texture estimates by means of components. *Z Metallkd* 1994;85:545–53.
- [19] ILOG, 1997–2004. Ilog, inc., CPLEX. Available from: <http://www.ilog.com/products/cplex/>.
- [20] Kocks U, Kallend J, Biondo A. Accurate representation of general textures by a set of weighted grains. *Text Microstruct* 1991;14–18:199–204. *iCOTOM 9, Special Issue*.
- [21] Kocks U, Tome C, Wenk H. *Texture and anisotropy: preferred orientations in polycrystals and their effect on materials properties*. Cambridge: Cambridge University Press; 1998.
- [22] Lücke K, Pospiech J, Jura J, Hirsch J. On the representation of orientations distribution functions (codfs) by model functions. *Z Metallkd* 1986;77:312–21.
- [23] Mardia K, Jupp P. *Directional statistics*. New York, NY: John Wiley & Sons Ltd.; 2000.
- [24] Markowitz H. Portfolio selection. *J Finance* 1952;7:77–91.
- [25] Mathur K, Dawson P. On modeling the development of crystallographic texture in bulk forming processes. *Int J Plast* 1989;5:67–94.
- [26] Matthies S. Standard functions in texture analysis. *Phys Stat Sol B* 1980;101:K111–5.
- [27] Matthies S, Muller J, Vinel G. On the normal distribution in the orientation space. *Text Microstruct* 1988;10:77–96.
- [28] Miehe C, Schröder J, Schotte J. Computational homogenization in finite plasticity. Simulation of texture development in polycrystalline materials. *Comp Meth Appl Mech Eng* 1999;171:387–418.
- [29] Padberg M. On the facial structure of set packing polyhedra. *Math Program* 1973;5:199–215.
- [30] Raabe D, Roters F. Using texture components in crystal plasticity finite element simulations. *Int J Plast* 2004;20:339–61.
- [31] Roe R. Description of crystalline orientation of polycrystalline materials. III. General solution to pole figure inversion. *J Appl Phys* 1965;36:2024–31.
- [32] Schaeben H. “Normal” orientation distribution. *Text Microstruct* 1992;19:197–202.
- [33] Schaeben H. *Diskrete mathematische Methoden zur Berechnung und Interpretation von kristallographischen Orientierungsdichten*. Oberursel: DGM Informationsgesellschaft; 1994.
- [34] Tarasiuk J, Wierzbanski K, Bacroix B. Texture decomposition into gauss-shaped functions: classical and genetic algorithm methods. *Computat Mater Sci* 2004;29:179–86.
- [35] Taylor G. Plastic strain in metals. *J Inst Metals* 1938;62:307–24.
- [36] Toth L, Van Houtte P. Discretization techniques for orientation distribution functions. *Text Microstruct* 1992;19:229–44.
- [37] Van Houtte P. A comprehensive mathematical formulation of an extended Taylor-Bishop-Hill model featuring relaxed constraints, the Renouard-Winterberger theory and a strain rate sensitive model. *Text Microstruct* 1988;8(9):313–50.
- [38] Wasserman G, Grewen J. *Texturen metallischer Werkstoffe*. Berlin: Springer; 1962.